ORGANOMETALLICS

Article

Cite This: *Organometallics* 2018, 37, 337−342

CO_2 Reduction Pathways on MnBr(N-C)$(CO)_3$ Electrocatalysts

Jonathon E. Vandezande[†] and Henry F. Schaefer, III*

Center for Computational Quantum Chemistry, University of Georgia, Athens, Georgia 30602, United States

Supporting Information

ABSTRACT: MnBr(*N*-ethyl-*N*′-2-pyridylimidazol-2-ylidine)$(CO)_3$ reduces CO_2 to CO in the absence of strong acids. Herein, we employ density functional theory and domain based local pair natural orbital coupled cluster theory to perform the first mapping of the catalytic pathway for this catalyst and various derivatives. The benzimidazole-containing derivative proceeds along the same pathway as its parent complex, but with an increased barrier to H^+ reduction. The phenolated complex shows barrierless CO_2 addition to the activated catalyst and facile C−O bond cleavage. All species exhibit a novel pyridine dissociation upon one-electron reduction of the tetracarbonyl species, but the active tricarbonyl catalysts can be regenerated with a small barrier. This novel step in the pathway presents a further consideration in the design of catalysts and provides insight into the potential degradation pathways of this catalyst.

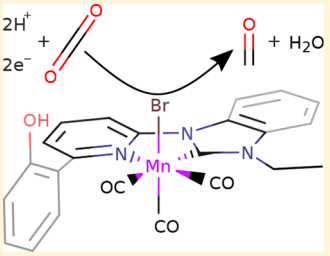

INTRODUCTION

Carbon dioxide (CO_2) is a persistent greenhouse gas and major contributor to anthropogenic climate change.[1] Significant research and development have been dedicated to capturing CO_2, with particular interest focused on enhancing the capture of CO_2 from coal plant emissions, as coal plants account for 76% of all global CO_2 power plant emissions.[1,2] The process of carbon capture could be made economically viable if the captured CO_2 was converted into a valuable product, as opposed to being sequestered.[3] However, CO_2 is relatively inert due to its highly oxidized nature, making it particularly difficult to efficiently transform.[4] Recent advances in catalyst design coupled with the falling cost of clean energy has made the use of CO_2 more attractive as a feedstock for commodity chemical production.[3,4] Particular interest has focused on converting CO_2 to CO as a step in the process of generating petrochemicals.[3,4]

Many homogeneous CO_2-reducing catalysts have been reported,[5−9] but they tend to suffer from a combination of high cost, low efficiency, low turnover frequency, and short lifetimes.[9] The well characterized ReCl(bpy)$(CO)_3$ (bpy = 2,2′-bipyridine) electrocatalyst reduces CO_2 with excellent selectivity for CO production over hydrogen formation.[10,11] As an alternative to expensive catalysts containing precious metals (e.g., Re, Pt, and Pd), inexpensive transition-metal catalysts, many including 3d transition metals, have been proposed.[8] Recent research by Bourrez et al.[5] showed that the electrocatalyst MnBr(bpy)$(CO)_3$, an analogue of ReCl(bpy)-$(CO)_3$, reduces CO_2 in MeCN at −1.70 V vs SCE. Relative to its Re analogue, this is a 0.4 V reduction in the overpotential (the excess potential above the theoretical minimum that is necessary to drive the reaction).

Various modifications to the MnBr(bpy)$(CO)_3$ catalyst have been suggested in an effort to increase the catalytic activity and reduce the overpotential. Bulky peripheral groups on the bipyridine have been used to inhibit dimerization, with *tert*-butyl groups in the 4- and 4′-positions[12] and mesityl groups in the 6- and 6′-positions[13] increasing the catalytic activity. Zeng et al. substituted isopropyldiazabutadiene for the bipyridine ligand,[14] shifting the initial reduction 0.3 V less negative in comparison to the original MnBr(bpy)$(CO)_3$ catalyst, but the catalytic activity is shifted 0.1 V more negative. Many other substitutions have been suggested with varying success: (1) wholesale substitution of bipyridine with phenanthroline[15] or mesityldiazabutadiene,[16] (2) substitution of the axial bromine for CN and NCS,[17,18] or (3) inclusion of Lewis acidic manganese atoms.[19] Several groups[20,21] have added a pendant phenol in order to allow for intramolecular proton donation that lowers the transition state of the rate-limiting step and increases the turnover frequency. Still others have substituted an N-heterocyclic carbene (NHC) for one of the pyridines, which maintains selectivity while lowering the necessary overpotential.[17,22]

This research endeavors to examine the catalytic pathways of MnBr(N-C)$(CO)_3$ catalysts (N-C = *N*-ethyl-*N*′-2-pyridylimidazol-2-ylidine, *N*-ethyl-*N*′-2-pyridylbenzimidazol-2-ylidine, 6-(2-hydroxyphenol)-*N*-ethyl-*N*′-2-pyridylimidazol-2-ylidine) (Figure 1). An understanding of the mechanism and potential degradation pathways of a catalyst is exceedingly important in guiding future catalyst design.[8,17,23] Various attempts have been made to elucidate the reduction pathways for the analogous MnBr(bpy)$(CO)_3$,[24] the corresponding Re catalyst,[25,26] and the phenol-containing MnBr(6-(2-hydroxyphenol)-2,2′-bipyridine)$(CO)_3$.[20] The pathways of these catalysts are similar, with a few important differences. The pathways begin with a two-electron reduction of the catalyst, liberating the coordinated halide. Next, CO_2 binds to the metal; this process is exergonic for Re(bpy)$(CO)_3$, while for the Mn analogue the binding is slightly endergonic. This species can only be reduced

Received: October 5, 2017
Published: January 31, 2018

DOI: 10.1021/acs.organomet.7b00743
Organometallics 2018, 37, 337−342

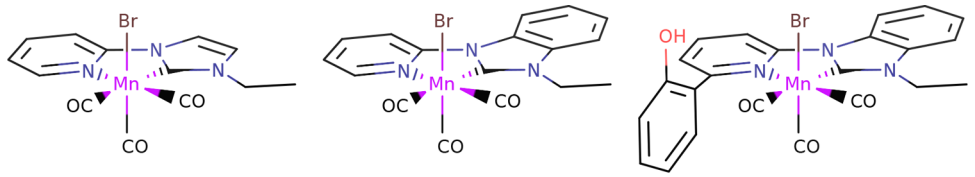

Figure 1. $Mn(N\text{-}C)(CO)_3$ catalysts studied herein.

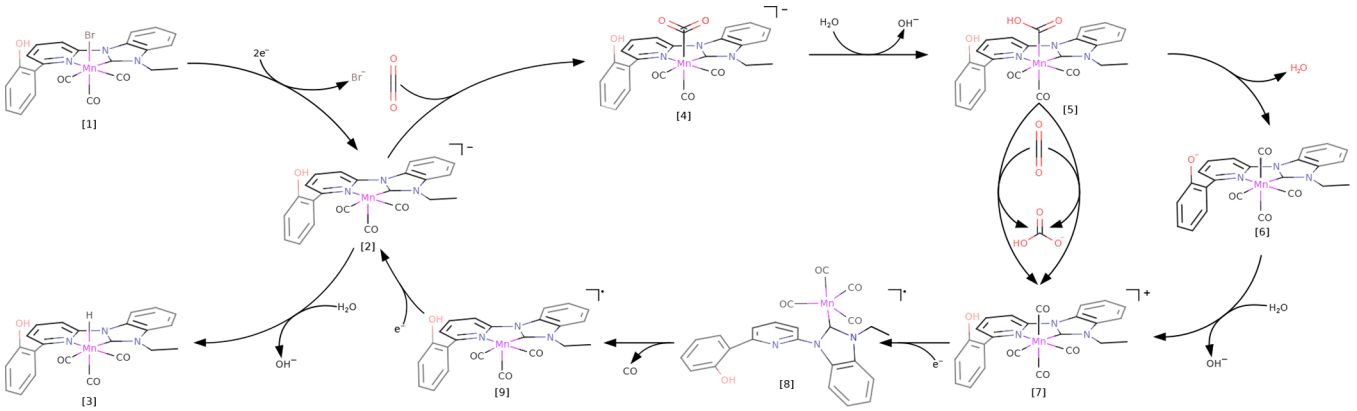

Figure 2. Proposed catalytic cycle of $MnBr(N\text{-}C)(CO)_3$ catalyst. This mirrors the catalytic cycle of $MnBr(bpy)(CO)_3$ with the addition of intermediate [**8**].

at highly negative potentials (computed to be −1.87 and −2.03 V vs SCE for $Re(CO_2)(bpy)(CO)_3^-$ and $Mn(CO_2)(bpy)(CO)_3^-$);[27] thus, protonation of this species is typically the preferred route. There are then two possible pathways, a reduction-first pathway and a protonation-first pathway. If electronegative groups are added to the ligands of the catalyst[28,29] or a significantly negative potential is applied,[24,25,27] the reduction-first pathway is preferred. The use of strong acids and nearby methoxy groups can encourage the protonation-first pathway.[30] If an exceedingly weak acid such as water is used for the protonation, the catalytic activity is significantly lowered.[12] However, catalytic activity has been shown using H_2O in the absence of a hard acid,[22] necessitating an alternative, such as using CO_2 to remove the OH^-.[20,26] Furthermore, if a pendant phenol is added near the active site, intramolecular proton donation can also be used for proton-mediated C−O bond cleavage, reducing the activation energy barrier.[20,21] If the CO remains bound to the catalyst after formation, a further reduction releases it, regenerating the bare catalyst.

The uniqueness of the NHC moiety notwithstanding, the $MnBr(N\text{-}C)(CO)_3$ catalysts are presumed to follow pathways similar to those of their $MnBr(bpy)(CO)_3$ counterpart. This paper endeavors to examine these catalytic pathways, elucidate the differences between the imidazole and benzimidazole reduction profiles, explore degradation pathways, and examine the effects of a pendant phenol on the catalytic cycle.

METHODS

Computational Methods. Initial computations were performed with density functional theory (DFT) as implemented in Orca 3.0.3.[31] These computations employed B3LYP,[32−34] the LANL08(f) ECP and basis set[35,36] for Mn (subsuming 10 electrons), and the 6-31++G**[37,38] basis set for all other atoms. The conductor-like screening model (COSMO)[39] was used to implicitly model acetonitrile (ϵ = 36.6). RIJCOSX[40] along with the assigned auxiliary basis sets was used to accelerate the Fock build step in all computations.

To refine the barrier heights, single-point electronic energies were determined using DLPNO-CCSD(T).[41] These computations employed the cc-pVTZ[42] basis set, the LANL08(f) ECP and basis set for Mn, the cc-pVTZ-JKFIT auxiliary basis set,[43] and COSMO for acetonitrile. Since DLPNO-CCSD(T) was only implemented in Orca 3.0.3 for an RHF reference, only the closed-shell species were studied by this method, precluding the study of one-electron reductions and open-shell reactions. The rate-limiting C−O heterolytic bond cleavage in the reaction $Mn(COOH)(bpy)(CO)_3 + CO_2 \rightarrow n(bpy)(CO)_4^+ + CO_3H^-$ is composed of closed-shell species and thus amenable to treatment by DLPNO-CCSD(T). The Gibbs free energy was then determined with the DLPNO-CCSD(T)/cc-pVTZ/LANL08(f)/COSMO(acetonitrile) electronic energies and B3LYP/6-31++G**/LANL08(f)/COSMO(acetonitrile) harmonic vibrational frequencies, employing the rigid rotor and harmonic oscillator approximations for the entropic contributions. To check for multireference character, and thus the applicability of single reference methods, MP2 natural orbitals were computed using RI-MP2 and the LANL08(f) and cc-pVTZ basis sets.

To ensure that transition states connected reactants and products, intrinsic reaction coordinate (IRC) computations were performed using GAMESS (2013).[44] All GAMESS computations employed B3LYP/6-31++G**/LANL08(f) as in the previous geometry optimizations but lack the implicit solvent model due to the inability of GAMESS to optimize with it. Transition states for the IRCs were reoptimized in GAMESS, featuring minimal changes in the geometry. All Mayer bond order computations were computed using ORCA 3.0.3.[31] All natural population analysis (NPA) computations were performed using NBO 6.0.[45]

RESULTS AND DISCUSSION

Initial Reduction. The catalytic cycles (Figure 2) for the imidazole (Im) and benzimidazole (BI) complexes are presumed to be similar to those for the $MnBr(bpy)(CO)_3$ and $ReCl(bpy)(CO)_3$ complexes,[24,25] with a few unique differences. The bipyridine catalyst has two experimentally determined one-electron-reduction potentials at −1.63 and −1.84 V vs Fc/Fc^+ in MeCN.[5] Meanwhile, the imidazole and benzimidazole ligands have concerted two-electron reductions

DOI: 10.1021/acs.organomet.7b00743
Organometallics 2018, 37, 337−342

Table 1. Properties of Imidazole (Im)- and Benzimidazole (BI)-Containing Catalysts (CO Stretches in cm^{-1})[a]

	charge			CO stretch		
	C	Mn	bond order	ν_a	ν_b	ν_c
Im	0.228	−0.590	0.62	1987	1896	1879
BI	0.264	−0.588	1.20	1989	1901	1882
Δ	0.036	0.002	0.58	2	5	3

[a]The natural population analysis (NPA) charges show increased accepting ability of the carbene carbon bonded to the Mn along with a decrease in electron density on the Mn. The Mayer bond orders show increased Mn−C back-bonding between the metal and benzimidazole. The increase in computed stretching frequencies indicates a decrease in the electron density on the Mn. These all lead to an observed increase in the reduction potential.

which occur at −1.91 and −2.01 V vs Fc/Fc^+, a shift of 0.10, which compares favorably to our theoretically computed shift of 0.12 V.[17] The change from two separate one-electron reductions to a concerted two-electron reduction is indicative of new processes appearing. After one-electron reduction, the Br^- dissociates on the catalysts and the carbonyl ligands rearrange to form a pseudo-trigonal-bipyramidal shape around the Mn. This new arrangement results in a lowering of the energy of the singly occupied $d_{x^2-y^2}$ orbital, allowing facile reduction of the catalyst.

The less negative shift in the reduction potential from imidazole to benzimidazole may be attributed to an increase in the back-bonding of the benzimidazole complex relative to the imidazole, leading to a decrease in electron density on the Mn.[22] Indeed, NPA calculations (Table 1) of the catalyst (species 1) show decreased electron density on the benzimidazole carbon coordinated to the Mn relative to the coordinating carbon on imidazole. The increase in π acidity is also evident in the increased Mn−C back-bonding, as illustrated by the increase in bond order (Table 1). The decrease in

Table 2. CO_2 vs H^+ Binding for Imidazole (Im)-, Benzimidazole (BI)-, and Phenol-imidazole (P-Im)-Containing Catalysts (See Figure 3), Referenced to the Energy of the Reactants, ΔG (kcal mol^{-1})[a]

	Im	BI	P-Im
	(a) CO_2 Binding		
TS	10.6	10.0	barrierless
final	3.1	8.0	−4.2
	(b) H^+ Binding		
TS	30.5	34.2	9.0
final	16.4	22.6	−11.5

[a]The transition state and final energy are referenced to the starting energy of the reactants at infinite separation. CO_2 binding is strongly preferred, even with the addition of a pendant phenol.

Table 3. First Protonation of Carboxylato [4] → [5] (see Figure 2) for Imidazole (Im)-, Benzimidazole (BI)-, and Phenol-imidazole (P-Im)-Containing Catalysts, Referenced to the Reactants, ΔG (kcal mol^{-1})[a]

IM	BI	P-Im (inter)	P-Im (intra)	P-Im (phenol)
22.8	25.2	32.0	0.9	31.1

[a]This is a barrierless or nearly barrierless process for all paths. The phenol may be used to protonate the carboxylato (P-Im (intra)), but the phenol itself must be regenerated (P-Im (phenol)), resulting in the same net increase in energy.

electron density of the carbon bonded to the Mn may be attributed to the formation of a Clar sextet[46] in the benzenoid ring of benzimidazole, which disrupts aromatic delocalization in the five-membered imidazolic moiety. This leaves less electron density on the carbene carbon and allows for a concomitant increase in back-bonding from the Mn, thus decreasing the electron density on the Mn atom and its surrounding ligands. This increase in back-bonding is not enough to make up for the

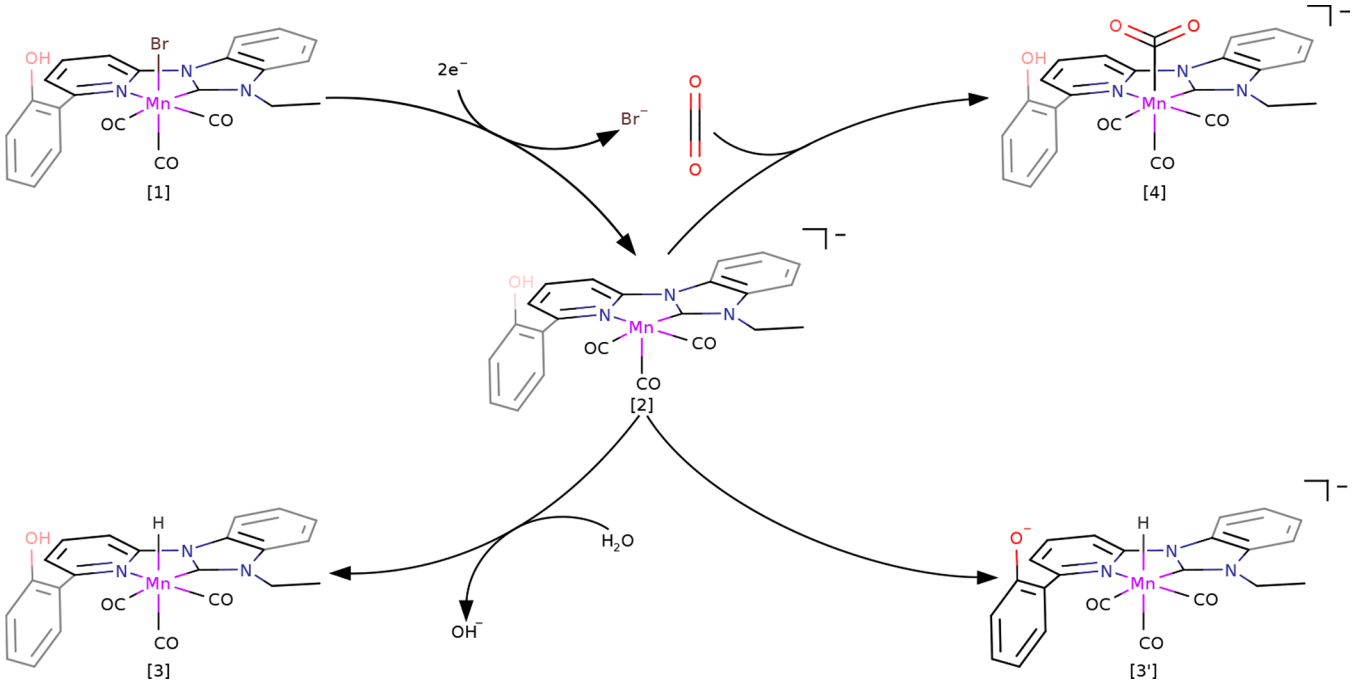

Figure 3. Proton vs CO_2 binding pathways. CO_2 is strongly preferred over H^+, but the addition of a pendant phenol lowers the barrier for both (Table 2). Step [2] → [3] is an intramolecular proton donation and thus happens much more readily than protonation from the water in solution.

DOI: 10.1021/acs.organomet.7b00743
Organometallics 2018, 37, 337−342

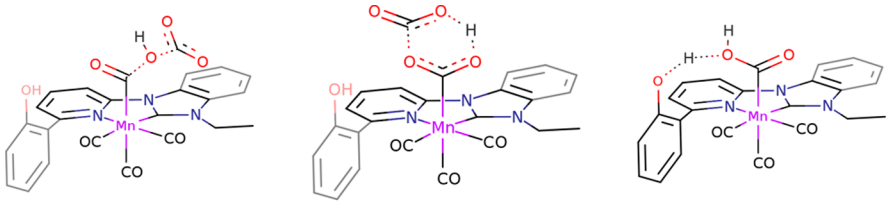

(a) TS 1 (b) TS 2 (c) TS 3

Figure 4. C−O bond cleavage steps [5] → [7] (TS 1 and TS 2) and [5] → [6] (TS 3) (see Figure 2 and Table 4).

Table 4. C−O Bond Cleavage Step ([5] → [7] and [5] → [6]), Referenced to the Energy of the Reactants, Δ*G* (kcal mol^{-1})[a]

		Im	BI	P-Im
		(a) Method 1		
TS	1	31.9	33.7	35.0
	2	23.2	24.4	21.5
	3			8.7
final	1 and 2	−4.0	−2.9	−3.3
	3			1.0
		(b) Method 2		
TS	1	30.4	29.3	30.4
	2	22.0	20.5	22.6
	3			7.0
final	1 and 2	0.1	0.5	1.4
	3			−5.3

[a]Method 1 uses the B3LYP energies, while method 2 employs DLPNO-CCSD(T) electronic energy corrections (see Methods for details). The bond cleavage can be mediated by either CO_2 (TS 1 and 2) or the pendant phenol (TS 3); see Figure 4. The intramolecular proton donation provided by the pendant phenol significantly lowers the barrier to C−O bond cleavage.

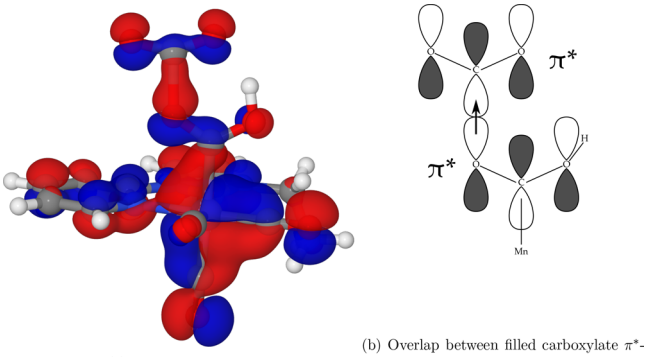

(a) HOMO−1 orbital (b) Overlap between filled carboxylate π*-orbital and empty attacking CO_2 π*-orbital.

Figure 5. Depection of orbital overlaps involved in TS 2 (see Figure 4b). The donation from the π* orbital of the carboxylate into the π* orbital of the attacking CO_2 stabilizes TS 2 and makes it lower in energy than TS 1, where no such interaction can occur.

decrease in electron delocalization into the carbene p orbital, as shown by natural population analysis (NPA) computations in Table 1. Theoretical and experimental[22] CO stretching frequencies also agree (Table 1), showing higher stretching frequencies with benzimidazole, indicating less electron donation from the Mn to the carbonyl π* orbitals.

Proton vs CO_2 Binding. Once the active catalyst has been generated by two-electron reduction and Br^- dissociation of the starting compound, there is an open coordination site for CO_2 binding (Figure 3). Previous Mn- and Re-based CO_2 reducing

Table 5. Thermal Entropy Contributions (−*T*Δ*S* kcal mol^{-1}) to the Gibbs Free Energy Barrier for the C−O Bond Cleavage ([5] → [7] and [5] → [6]; See Figure 4), Referenced to the Thermal Entropy Contributions of the Reactants[a]

	TS	Im	BI	P-Im
vibrational	1	−5.1	−4.6	−5.1
	2	−2.3	−3.3	−1.7
	3			−1.9
rotational	1	3.7	3.7	3.7
	2	3.7	3.7	3.7
	3			0.0
translational	1	11.0	11.0	11.0
	2	11.0	11.0	11.1
	3			0.0

[a]Transition states TS 1 and TS 2 both have large entropic penalties due to the loss of rotational and translational freedom arising from the binding of a CO_2 from solution. TS 3 has no such barrier due to the use of intramolecular proton donation.

catalysts have shown a marked selectivity for CO_2 reduction to CO in comparison to proton reduction to H_2.[5,24] In $MnBr(bpy)(CO)_3$ complexes this has previously been attributed to a substantially higher barrier for proton coordination relative to CO_2 coordination.[24] Previous protonation mechanisms had a hard Lewis acid such as K^+ stabilizing the weak acid transition state.[24] If a softer electrolyte were to be used as a supporting electrolyte, such as tetrabutylammonium perchlorate (TBAP), the protonation pathway would become highly unfavorable. For $Mn(N\text{-}C)(CO)_3^-$, protonation with H_2O has a significantly higher barrier than CO_2 binding (Table 2), due to the high pK_a of H_2O in acetonitrile (computed pK_a 30.7 in acetonitrile[27]). The nature of the resulting products was confirmed to be the charged species $MnH(N\text{-}C)(CO)_3$ and OH^- by examination of the Löwdin charges of the products resulting from the IRC and relaxed surface scans. If stronger Brønsted acids are used, such as phenol and HCl, the protonation of the active complex will be more favorable, making hydrogen a competing product. When a pendant phenol is attached to the active catalyst (P-Im), CO_2 binding becomes barrierless due to hydrogen bonding from the alcohol. However, protonation is also significantly easier due to the lower pK_a and the intramolecular pathway, potentially leading to a competitive reduction of H^+ to H_2.

First Protonation. After the CO_2 has bound to the Mn in the previous step, the resulting carboxylate must be protonated. Previous studies with weak acids and K^+ have shown this step to proceed with a small barrier for the bipyridine analogue.[24] With water, in the absence of a supporting electrolyte, the process becomes significantly uphill due to the high pK_a of water in acetonitrile (Table 3). This reaction is an uphill

DOI: 10.1021/acs.organomet.7b00743
Organometallics 2018, 37, 337−342

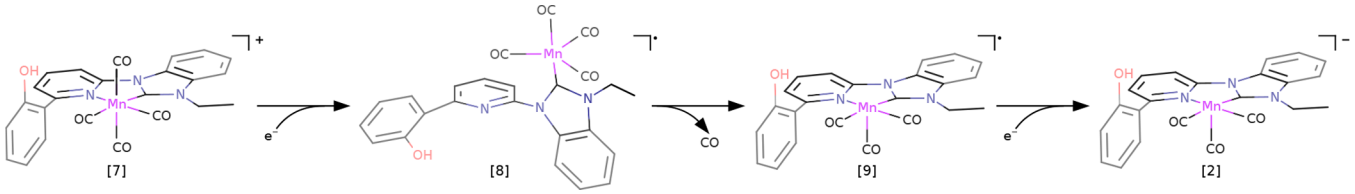

Figure 6. Regeneration of active catalyst by two-electron reduction and CO removal. The pyridine spontaneously unbinds from the Mn upon one-electron reduction but rebinds upon removal of the CO.

Table 6. Barrier to Liberation of CO in Step [8] → [9], Referenced to the Energy of the Reactants, ΔG (kcal mol^{-1})[a]

	IM	BI	P-Im
TS	5.6	7.9	11.3
final	−3.7	−3.7	1.9

[a]No DLPNO-CCSD(T) correction is included, as open-shell DLPNO is not implemented in ORCA 3.0.3.

process with no excess barrier, as demonstrated by potential energy scans in the Supporting Information. The inclusion of a pendant phenol increases the barrier to protonation with water, as it weakens the hydrogen bond between the phenol and the carboxylate. The pendant phenol can be used for the protonation of the carboxylate, in a nearly isoenergetic process (0.9 kcal mol^{-1}). The exact nature of the proton transfer from the pendant phenol is difficult to determine at this level of theory due to the low barrier. However, once this phenol has been used to protonate the carboxylate, the phenol must be reprotonated in a similarly barrierless process.

C−O Bond Cleavage. The C−O bond cleavage of the carboxylate group has previously been shown to be the rate-limiting step in CO_2 reduction with MnBr(bpy)(CO)$_3$. Previous mechanisms have shown that this bond breaking is induced by proton donation from a Brønsted acid. However, H_2O is too weak of an acid (computed pK_a = 30.7 in MeCN) to be used as a proton source (especially in the absence of any stabilizing cations) and thus an alternative mechanism is necessary to explain the observed catalytic activity. Agarwal et al.[26] proposed a mechanism for the ReCl(bpy)(CO)$_3$ analogue whereby the readily available CO_2 in solution aids in the removal of the OH^-, generating bicarbonate. This bicarbonate will be a long-lived species and solution and may be a source of further protons; CO_2 will only be regenerated under significantly acidic conditions.

Removal of OH^- by CO_2 can proceed via two pathways. TS 1 illustrates a side-on attack of the carboxylate, transferring the OH^- moiety and producing HCO_3^- and CO (Figure 4a). The imidazole (Im), benzimidazole (BI), and imidazole with pendant phenol (P-Im) all show reaction barriers of greater than 30 kcal mol^{-1} (Table 4). Alternatively, TS 2 illustrates an approach of CO_2 from above (Figure 4b), with the occupied π^* orbital of the carboxylate donating into the unoccupied π^* orbital of the CO_2 (Figure 5). Due to this increased electronic stabilization, TS 2 has a 21 kcal mol^{-1} barrier that is 9 kcal mol^{-1} lower than TS 1.

As an alternative to the intermolecular pathways, intramolecular proton transfer from a pendant phenol in P-Im is possible (Figure 4c). Such a mechanism avoids the loss of rotational and translational entropy upon association of CO_2, thus leading to a lower energy barrier. As shown in Table 4, this pathway has an energy barrier of 7.0 kcal mol^{-1}, 15 kcal mol^{-1} lower than the lowest barrier for the intermolecular pathways. The intermolecular pathways show large translational and rotational entropy penalties for the transition states (Table 5), whereas the intramolecular pathway does not show such penalties, accounting for much of the decrease in barrier height for the intramolecular pathway.

Regeneration. Once the OH^- is removed, species [7] can be reduced, causing the pyridine ligand to spontaneously unbind from the Mn, forming [8] (see Figure 6). This significant rearrangement hinders accurate computational determination of the reduction potential, as the relaxation inhibits determination of the Gibbs free energy difference due to the reduction. To ensure that dispersion effects would not prevent this unbinding, exploratory B3LYP-D3/def2-svp computations were performed on these species, and the same spontaneous unbinding of the pyridine upon reduction was observed. The subsequent barrier to CO removal and ligand recombination (forming species [9]) is small (Table 6), indicating that species [8] is only a transient species in solution. Species [9] can then be reduced again to re-form the active catalyst, species [2].

CONCLUSION

We have elucidated the reduction pathway of CO_2 to CO on MnBr(N-C)(CO)$_3$ for three N-heterocyclic carbene containing N−C ligands. Our results are generally consistent with previous experimental work on MnBr(N-C)(CO)$_3$ catalysts and expand on previous studies on CO_2 reduction with Mn(I) tricarbonyl compounds.[20,24] These results reveal avenues for future modifications of CO_2-reducing catalysts to improve the turnover frequency and turnover number. In particular, since CO_2 binding is strongly preferred over H^+ binding, even with the inclusion of a pendant phenol, stronger acids could safely be used without significantly increasing H_2 production. The use of CO_2 for removal of the OH^- is shown to allow reduction of CO_2 in the absence of hard-acid electrolytes, with H_2O as the only proton source. Furthermore, the inclusion of a pendant phenol near the active site was shown to dramatically decrease the barriers to the C−O bond cleavage step of the catalytic pathway and is predicted to yield an increased turnover frequency. When the tetracarbonyl species is reduced, dissociation of the pyridine moiety is observed, potentially leading to a catalyst degradation pathway. Investigation and prevention of this dissociation remains an avenue of further study in order to improve the turnover number.

ASSOCIATED CONTENT

Supporting Information

The Supporting Information is available free of charge on the ACS Publications website at DOI: 10.1021/acs.organomet.7b00743.

DOI: 10.1021/acs.organomet.7b00743
Organometallics 2018, 37, 337−342

Structures of all the computed species along with their energies, vibrational frequencies, charge, multiplicity, etc. (PDF)

All computed molecule Cartesian coordinates (XYZ)

AUTHOR INFORMATION

Corresponding Author

*E-mail for H.F.S.: ccq@uga.edu.

ORCID

Jonathon E. Vandezande: 0000-0001-7969-5498

Henry F. Schaefer III: 0000-0003-0252-2083

Present Address

†J.E.V.: Max Planck Institute for Coal Research, Mülheim an der Ruhr 45470, Germany.

Notes

The authors declare no competing financial interest.

ACKNOWLEDGMENTS

The authors thank Dr. Jay Agarwal for his many helpful conversations fundamental to the research herein. This work has been supported by the National Science Foundation Grant No. CHE-1661604.

REFERENCES

(1) Metz, B.; Davidson, O.; de Coninck, H.; Loos, M.; Meyer, L. *IPCC Special Report on Carbon dioxide Capture and Storage*; Cambridge University Press: Cambridge, U.K., 2005.

(2) Haszeldine, R. S. *Science (Washington, DC, U. S.)* **2009**, *325*, 1647−1652.

(3) Olah, G. A.; Goeppert, A.; Prakash, G. K. S. *J. Org. Chem.* **2009**, *74*, 487−498.

(4) Centi, G.; Quadrelli, E. A.; Perathoner, S. *Energy Environ. Sci.* **2013**, *6*, 1711−1731.

(5) Bourrez, M.; Molton, F.; Chardon-Noblat, S.; Deronzier, A. *Angew. Chem., Int. Ed.* **2011**, *50*, 9903−9906.

(6) Leitner, W. *Coord. Chem. Rev.* **1996**, *153*, 257−284.

(7) Wang, W.-H.; Himeda, Y.; Muckerman, J. T.; Fujita, E. *Adv. Inorg. Chem.* **2014**, *66*, 189−222.

(8) Qiao, J.; Liu, Y.; Hong, F.; Zhang, J. *Chem. Soc. Rev.* **2014**, *43*, 631−675.

(9) Cokoja, M.; Bruckmeier, C.; Rieger, B.; Herrmann, W. A.; Kühn, F. E. *Angew. Chem., Int. Ed.* **2011**, *50*, 8510−8537.

(10) Hawecker, J.; Lehn, J.-M.; Ziessel, R. *J. Chem. Soc., Chem. Commun.* **1983**, *1*, 536−538.

(11) Sullivan, B. P.; Bolinger, C. M.; Conrad, D.; Vining, W. J.; Meyer, T. J. *J. Chem. Soc., Chem. Commun.* **1985**, *20*, 1414−1416.

(12) Smieja, J. M.; Sampson, M. D.; Grice, K. A.; Benson, E. E.; Froehlich, J. D.; Kubiak, C. P. *Inorg. Chem.* **2013**, *52*, 2484−2491.

(13) Sampson, M. D.; Nguyen, A. D.; Grice, K. A.; Moore, C. E.; Rheingold, A. L.; Kubiak, C. P. *J. Am. Chem. Soc.* **2014**, *136*, 5460−5471.

(14) Zeng, Q.; Tory, J.; Hartl, F. *Organometallics* **2014**, *33*, 5002−5008.

(15) Kurtz, D. A.; Dhakal, B.; Hulme, R. J.; Nichol, G. S.; Felton, G. A. N. *Inorg. Chim. Acta* **2015**, *427*, 22−26.

(16) Vollmer, M. V.; Machan, C. W.; Clark, M. L.; Antholine, W. E.; Agarwal, J.; Schaefer, H. F.; Kubiak, C. P.; Walensky, J. R. *Organometallics* **2015**, *34*, 3−12.

(17) Agarwal, J.; Stanton, C. J.; Shaw, T. W.; Vandezande, J. E.; Majetich, G. F.; Bocarsly, A. B.; Schaefer, H. F. *Dalt. Trans.* **2015**, *44*, 2122−2131.

(18) Machan, C. W.; Stanton, C. J.; Vandezande, J. E.; Majetich, G. F.; Schaefer, H. F.; Kubiak, C. P.; Agarwal, J. *Inorg. Chem.* **2015**, *54*, 8849−8856.

(19) Sampson, M. D.; Kubiak, C. P. *J. Am. Chem. Soc.* **2016**, *138*, 1386−1393.

(20) Agarwal, J.; Shaw, T. W.; Schaefer, H. F.; Bocarsly, A. B. *Inorg. Chem.* **2015**, *54*, 5285−5294.

(21) Franco, F.; Cometto, C.; Ferrero Vallana, F.; Sordello, F.; Priola, E.; Minero, C.; Nervi, C.; Gobetto, R. *Chem. Commun.* **2014**, *50*, 14670−14673.

(22) Agarwal, J.; Shaw, T. W.; Stanton, C. J.; Majetich, G. F.; Bocarsly, A. B.; Schaefer, H. F. *Angew. Chem., Int. Ed.* **2014**, *53*, 5152−5155.

(23) White, J. L.; Baruch, M. F.; Pander, J. E.; Hu, Y.; Fortmeyer, I. C.; Park, J. E.; Zhang, T.; Liao, K.; Gu, J.; Yan, Y.; Shaw, T. W.; Abelev, E.; Bocarsly, A. B. *Chem. Rev.* **2015**, *115*, 12888−12935.

(24) Riplinger, C.; Sampson, M. D.; Ritzmann, A. M.; Kubiak, C. P.; Carter, E. A. *J. Am. Chem. Soc.* **2014**, *136*, 16285−16298.

(25) Keith, J. A.; Grice, K. A.; Kubiak, C. P.; Carter, E. A. *J. Am. Chem. Soc.* **2013**, *135*, 15823−15829.

(26) Agarwal, J.; Sanders, B. C.; Fujita, E.; Schaefer, H. F.; Harrop, T. C.; Muckerman, J. T. *Chem. Commun.* **2012**, *48*, 6797−67979.

(27) Riplinger, C.; Carter, E. A. *ACS Catal.* **2015**, *5*, 900−908.

(28) Stanton, C. J.; Machan, C. W.; Vandezande, J. E.; Jin, T.; Majetich, G. F.; Schaefer, H. F.; Kubiak, C. P.; Li, G.; Agarwal, J. *Inorg. Chem.* **2016**, *55*, 3136−3144.

(29) Stanton, C. J.; Vandezande, J. E.; Majetich, G. F.; Schaefer, H. F.; Agarwal, J. *Inorg. Chem.* **2016**, *55*, 9509−9512.

(30) Ngo, K. T.; McKinnon, M.; Mahanti, B.; Narayanan, R.; Grills, D. C.; Ertem, M. Z.; Rochford, J. *J. Am. Chem. Soc.* **2017**, *139*, 2604−2618.

(31) Neese, F. *Wiley Interdiscip. Rev. Comput. Mol. Sci.* **2012**, *2*, 73−78.

(32) Lee, C.; Yang, W.; Parr, R. G. *Phys. Rev. B: Condens. Matter Mater. Phys.* **1988**, *37*, 785−789.

(33) Becke, A. D. *J. Chem. Phys.* **1993**, *98*, 5648−5652.

(34) Becke, A. D. *J. Chem. Phys.* **1996**, *104*, 1040−1046.

(35) Hay, P. J.; Wadt, W. R. *J. Chem. Phys.* **1985**, *82*, 270−283.

(36) Roy, L. E.; Hay, P. J.; Martin, R. L. *J. Chem. Theory Comput.* **2008**, *4*, 1029−1031.

(37) Krishnan, R.; Binkley, J. S.; Seeger, R.; Pople, J. A. *J. Chem. Phys.* **1980**, *72*, 650−654.

(38) McLean, A. D.; Chandler, G. S. *J. Chem. Phys.* **1980**, *72*, 5639−5648.

(39) Klamt, A.; Schüürmann, G. *J. Chem. Soc., Perkin Trans. 2* **1993**, *2*, 799−805.

(40) Neese, F.; Wennmohs, F.; Hansen, A.; Becker, U. *Chem. Phys.* **2009**, *356*, 98−109.

(41) Riplinger, C.; Neese, F. *J. Chem. Phys.* **2013**, *138*, 034106.

(42) Dunning, T. H. *J. Chem. Phys.* **1989**, *90*, 1007−1023.

(43) Weigend, F.; Köhn, A.; Hättig, C. *J. Chem. Phys.* **2002**, *116*, 3175−3183.

(44) Schmidt, M. W.; Baldridge, K. K.; Boatz, J. A.; Elbert, S. T.; Gordon, M. S.; Jensen, J. H.; Oseki, S. K.; Matsunaga, N.; Nguyen, K. A.; Su, S.; Windus, T. L.; Dupuis, M.; Montgomery, J. A. *J. Comput. Chem.* **1993**, *14*, 1347−1363.

(45) Glendening, E. D.; Landis, C. R.; Weinhold, F. *J. Comput. Chem.* **2013**, *34*, 1429−1437.

(46) Solà, M. *Front. Chem.* **2013**, *1*, 1−8.

DOI: 10.1021/acs.organomet.7b00743
Organometallics 2018, 37, 337−342